Journal of Materials Chemistry A

Accepted Manuscript

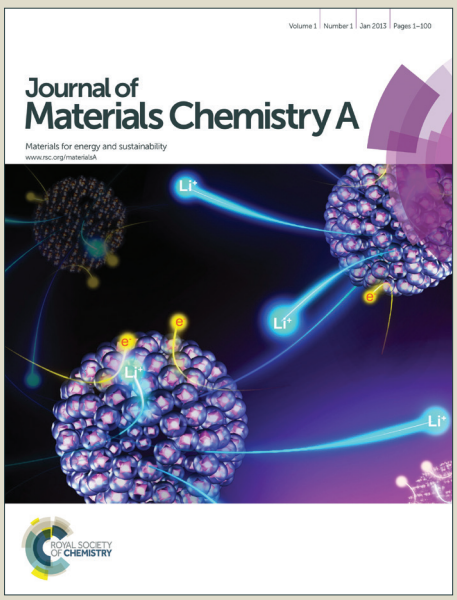

ROYAL SOCIETY OF CHEMISTRY

www.rsc.org/materialsA

Journal of Materials Chemistry A

ARTICLE TYPE

Cite this: DOI: 10.1039/c0xx00000x

www.rsc.org/xxxxxx

Nitrogen-rich porous carbon derived from biomass as a high performance anode material for lithium ion batteries

Junke Ou,[a] Yongzhi Zhang,[b] Li Chen,[c] Qian Zhao,[a] Yan Meng,[a] Yong Guo*[c] and Dan Xiao*[a,b,c]

Received (in XXX, XXX) Xth XXXXXXXXX 20XX, Accepted Xth XXXXXXXXX 20XX

DOI: 10.1039/b000000x

Nitrogen-rich porous carbon derived from ox horn has been successfully synthesized through an economically viable and an environmentally benign approach. Such an ox horn derived carbon (OHC) possesses a large surface area (BET surface area is 1300 m^2 g^{-1}), unique 3D porous nanostructure and high inherent nitrogen content (5.5%). The OHC, as an anode material for lithium ion batteries (LIBs), exhibits superior electrochemical performances, such as high reversible capacity (1181 mA h g^{-1} at the current density of 100 mA g^{-1}) and superior rate capability (304 mA h g^1 at 5 A g^{-1}). Furthermore, this study demonstrates the exploitation of a universal material in nature, viz., ox horn, as a potential anode for the most sought after energy storage application.

.

1. Introduction

With the depletion of fossil fuel resources and the global warming, developing a renewable energy storage system with high energy and power density becomes more and more urgent. Particularly, lithium ion batteries (LIBs) with high energy density, long cycle life, lack of memory effects, and flexible design are currently dominating the commercial market owing to the potential application of smart and portable electronic devices like mobile phones, laptops, camera, etc.[1] The performance of the rechargeable lithium ion batteries mainly depend upon the characteristics of the active materials employed in the electrodes. It is well known that graphite is the most popular commercial anode material for LIBs due to its low cost and low electrochemi cal potential with respect to lithium metal.[2, 3] However, the present lithium ion batteries using graphite with limited storage capacity of 372 mA h g^{-1} cannot meet requirements for more demanding applications with high energy and high power. Thus, much effort has been aimed at the exploration of novel carbon materials possessing high capacity, high rate capability, easy accessibility and environmental friendliness.[4]

Many carbonaceous anode materials with various structures have been investigated, such as carbon nanotube (CNT), carbon nanofibers (CNF), nanobeads, hollow nanospheres and graphene.[5-9] However, most of these synthesis methods require special equipments, special reagents or complex process control. Recently, as a renewable source, biomasses have received much attention for their promising applications in the preparation of carbonaceous materials because of rich raw materials and low cost. Therefore, carbonaceous materials derived from biomass as anode for LIBs have been explored with sources as diverse as cotton wool, coconut, starch, coffee shells, banana fibers, rice husk, rice straw, algae, cherry stones, pinecone hull and wheat straw.[10-20] Meanwhile, these biomass-derived carbons, especially nanostructured porous carbon materials, being a three-dimensional (3D) conductive network, are of particular interest in providing high lithiation capability and excellent cycling stability because the porous nanostructure can not only shorten the transport length for Li-ion but also offer large electrode/electrolyte interface for the charge-transfer reaction.[21-22]

Electrochemical performance of carbons can be further enhanced by surface functionalities (such as P, N and B).[23-25] The nitrogen (N) atoms, possessing a comparable atomic size and five valence electrons for bonding with carbon atoms, have been widely used for the doping of carbon-based materials. [24] The well-bonded N atom provides more active sites to increase the interaction between the carbon and adsorbents, thus it is expected to enhance electrochemical performance. However, incorporation of nitrogen into carbon matrix often involves the procedures of hydrothermal, ultrasonic and electrochemical approaches, which causes some challenges. Besides, use of toxic reagents results in severe environmental issues. In this point, preparation of nitrogen containing carbon from abundant naturally sources with ample amount of nitrogen seems more appealing, because the usage of toxic chemicals could be avoided. Recently, human hair was reported to prepare a heteroatom doped carbon material for supercapacitors and LIBs.[26-28] Another sample: N-doped

mesoporous carbon from protein was reported to exhibit an ultra-high capacity of 1780 mA h g^{-1} at a current density of 100 mA g^{-1}.[24] These samples showed the potential of biomass being used to fabricate carbon materials for energy storage and converse.

Ox horn, a unique natural composite material, is a promising raw material for preparing the nitrogen containing porous carbons. It is composed of mineral of calcium phosphate and organic of keratin.[29] Most common interest in horn is focused on its decoration and its medicine values, Few studies concerning its other applications are reported. The organic component of keratin provides the carbon and nitrogen for porous N-doped carbon materials. In addition, horn, a natural raw material from animal, is very cheap and environment friendly with abundant production, especially its application for fabrication of porous carbon materials will be quite advantageous.

Therefore, in this work, ox horn was reported to act as a novel, low-cost and easily available precursor for the synthesis of nitrogen containing carbon anode material. High specific surface area and porous structure of carbon have been achieved by KOH activation during carbonization. When evaluated as the anode material for lithium ion batteries, the obtained carbons from ox horn exhibit attractive electrochemical performances. To be specific, ox horn derived carbon (OHC) anode delivers excellent capacities of 1181, 750 and 304 mA h g^{-1} corresponding to current densities of 100 (0.26 C, 1C=372 mA g^{-1}), 500 (1.34 C) and 5000 mA g^{-1} (13.4 C) respectively. These results demonstrate that as-synthesized OHC is a promising electrode material for LIBs. To the best of our knowledge, this is the first time in literature to report: anode materials derived from ox horn for LIBs. Moreover, Compared with the surface chemical post-modification (for instance, porous carbon prepared by NH_3 treatment of at high temperature), our work provides a simple approach to produce a nitrogen-rich porous carbon.

2. Experimental section

2.1. Synthesis

All chemicals were of analytical grade and purchased from Tianjing Chemical Industrial Corp and used as received without further purification. To ensure the quality and consistency, ox horn was obtained from the same cow. A typical synthesis process was as follows.

2.1.1 Preparation of ox horn derived carbon material (OHC).

Preparation of OHC involves a simple approach as described below. The obtained ox horn was cut into small pieces by the grinder. The collected pieces were thoroughly washed with isopropanol and dried at 80 ℃. Then the dried sample was immersed in KOH solution (the amount of KOH to horn ratio in terms of weight was 3:1) for 24 h and dried in an oven at 120 ℃. The obtained substance was carbonized at 700 ℃ for 2 h in a horizontal tube furnace under Ar atmosphere with a heating ramp of 5 ℃ min^{-1}. The obtained black powder was washed with 1 M HCl to remove metal impurities and thoroughly washed with deionized water to ensure it was neutral. The resulting carbon material was dried at 70 ℃ under vacuum. Usually, ox horn (20 g) can yield about 2 g of porous carbons. The whole process needs about two days, including KOH solution immersing (one day), drying, calcination, washing and the final drying. The as-fabricated ox horn derived carbon material is denoted as OHC. For comparison, the dried ox horns without the KOH treatment were directly annealed at 700 ℃ for 2 hours under Ar flow and designated as NOHC.

2.2. Characterization of materials.

The obtained materials were subjected to various characterization techniques. X-ray powder diffraction (XRD) patterns of the products were estimated on a TD-3500 X-ray powder diffractometer (Tongda, China). Surface morphology of the sample was investigated using a Hitachi S4800 field emission scanning electron microscopy (FESEM). The transmission electron microscopy (TEM) images were carried out using a FEI Tecnai G2 20 TEM (Hillsboro, OR, USA). Raman spectrum was recorded using a confocal LabRAM HR800 spectrometer, HORIBA Jobin Yvon, France. X-ray photoelectron spectra (XPS) were recorded using a Kratos XSAM 800 spectrometer (Manchester,UK). Elemental analysis was done using a EuroEA3000 (Leeman, USA) Analyzer. Fourier transform infrared (FTIR) spectra were obtained with a PerkinElmer instrument (USA) using KBr pellet technique. Nitrogen sorption analysis was carried out with a micrometeretics tristar 3020 automatic analyzer (USA). The samples were degassed at 300 ℃ for 6 h before absorption measurements. Specific surface areas were estimated according to the BET model, and pore size distributions (PSDs) were calculated by applying the NLDFT method.

2.3. Electrochemical measurements

To evaluate the electrochemical performances of ox horn derived carbons, 2032-type coin cells were fabricated. The working electrode was fabricated by depositing the mixed slurry of active material, acetylene black and polyvinylidene fluoride (PVDF) binder in N-methyl pyrrolidinone (NMP) solvent with a weight ratio of 8 : 1 : 1 onto copper foil current collector, and then drying at 100 ℃ under vacuum for 2 hours. The mass loading of active material on each electrode was about 1.3 mg cm^{-2}. Lithium metal foil was used as a counter/reference electrode. Celgard 2400 microporous polypropylene film was used as the separator and the electrolyte was 1 M $LiPF_6$ dissolved in 1:1 v/v ethylene carbonate (EC): dimethyl carbonate (DMC). The cells were assembled in an argon-filled glove box (H_2O< 2 ppm, O_2< 0.5 ppm, Dellix, China). The galvanostatic charge/discharge tests were performed between 0.01-3.0 V (vs. Li^+/Li) at room temperature on a Newware CT-3008W battery cycler (Guangdong, China). Cyclic voltammetry (CV) measurements were carried out at a scanning rate of 0.1 mV s^{-1} on an Autolab PGSTAT 302 electrochemical workstation in the voltage range of 0.01-3.0 V. Electrochemical impedance spectroscopy (EIS) was taken in the frequency range 0.01-100 kHz at a charged stage with an applied amplitude of 5 mV.

3. Results and discussion

X-ray diffraction (XRD) patterns of the two samples were presented in Fig. 1a. Two peaks located at 2 Theta=23.6° and 43.6° can be assigned to the (002) and (100) reflections of carbon respectively, which indicates that the samples are predominantly made up of single-layer carbon sheets that are not stacked in a parallel fashion.[30] This amorphous structure is favorable for lithium ion intercalation and deintercalation.[31] As a measure of the number of carbon sheets arranged as single layers, Dahn used the empirical parameter (R), which is defined as the ratio of height of the (002) Bragg peak to the background.[32] It has been demonstrated that the R values decrease as the single layer contents in the carbon increase, and a smaller R value indicates a lower degree of the graphitization.[33] The R value of OHC (1.5) is smaller than that of NOHC (1.8), it reveals that activation by KOH may result in a lower degree of graphitization of the structure. The calculated d spacing value of (002) plane of OHC is 0.383 nm, which is higher than the pure graphitic carbon structure (0.335 nm). The larger (002) interlayer space would be beneficial for Li storage.[31] Raman spectra which have been widely applied to characterize carbon materials are sensitive to the slight structural changes. The Raman spectrum of two carbons shows two peaks at 1590 cm^{-1} (G band) and 1350 cm^{-1} (D band) (Fig. 1b), corresponding to the vibration in sp^2 band carbon atoms in a two-dimensional hexagonal lattice, and the defect and disorder-induced structures in the graphene layers of carbon materials.[34] It is well known that the intensity ratio of the I_D/I_G stands for disorder degree and the average size of the sp^2 domains.[31, 34, 35] After activation, the Raman spectra of OHC exhibits an increased intensity ratio of D-band to G band, I_D/I_G=1.02, significantly higher than that of NOHC (I_D/I_G=0.86). This result indicates that activation promotes the presence of defects and disordered sections, which can also be confirmed by XRD pattern (Fig.1a).

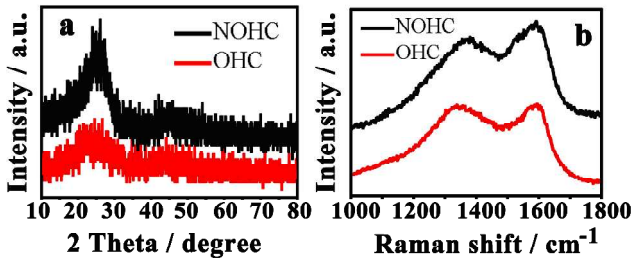

Fig.1 XRD pattern (a) and Raman spectra (b) of the two samples of NOHC and OHC.

In order to further examine the porous structure of OHC, the nitrogen adsorption–desorption isotherms were carried out (Fig. 2a). It can be clearly seen that the sample of NOHC presented a very low amount of adsorbed nitrogen, revealing a non-porous property, while the OHC showed a type I sorption isotherm with a much higher nitrogen sorption capacity, indicating the microporous property. The specific Brunauer–Emmett–Teller (BET) surface area of the KOH-activated porous carbon material can be up to 1300 m^2 g^{-1} with a pore volume of 0.63 cm^3 g^{-1}. In comparison, the specific BET surface area of the carbon material derived from ox horn without KOH treatment was about 10 m^2 $g^{-1}$and can be ignored. The pore size distributions (PSDs) for OHC were estimated by non-local density functional theory (NLDFT) and are shown in Fig. 2b. It is clear that the OHC is mainly composed of micropores between 1 and 2 nm. Although chemical activation usually results in the micropores in the surface, some mesopores located between 3 and 4 nm were still observed in Fig. 2b. The small amount of mesopores may be derived from the randomly arranged carbon sheets that are not stacked in parallel. It can be confirmed by the analysis of XRD pattern and Raman spectra (Fig. 1). In general, materials with high surface area and hierarchical pore structure will exhibit better electrochemical performance, especially in rate performances. Therefore, the currently fabricated OHC material is expected to act as a better anode material for lithium ion batteries.

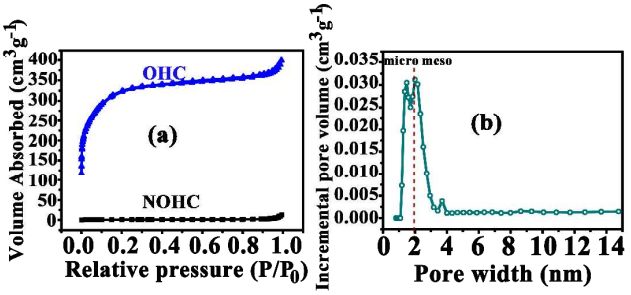

Fig.2 (a) Nitrogen adsorption–desorption isotherms of NOHC and OHC, (b) pore size distribution for OHC

Fig. 3 shows SEM images of ox horn, carbon material derived from ox horns, and carbon material derived from KOH-treated ox horns. As presented in Fig. 3a, the ox horns mainly comprised large and smooth bulk with small amount of ravines. After pyrolysis at 700 ℃ for 2 h in Ar, the obtained carbon material was broken into small sheets with different sizes (Fig. 3b). An image of enlargements showed that the surface of the carbon without KOH treatment was very smooth and with few pores (the inset of Fig. 3b). Fig. 3c displays that the KOH-activated carbon material has a more dispersed morphology than that without KOH treatment. Fig. 3d further reveals details of the morphology of KOH-activated carbon material. A large amount of nanoscale pores was observed, forming a three-dimensional (3D) connected porous structure.

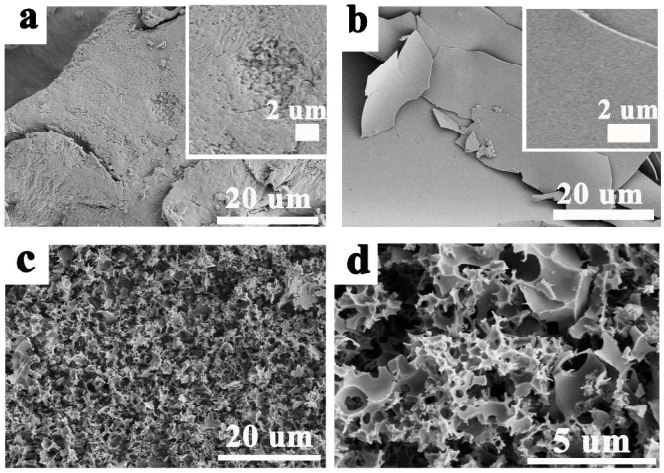

Fig.3 FESEM image of (a) ox horn; (b) carbon derived from ox horn without KOH treatment; (c and d) carbon derived from ox horn with KOH treatment; The insets of (a) and (b) are the partial enlargements of the relevant images.

OHC was further characterized using HRTEM, which was shown in Fig. 4 (a and b). HRTEM images clearly shows that the large quantities of micropores and channels were distributed in the material of OHC (with KOH treatment). The unique porous structures are ideal electrolyte diffusion channels and this interconnection feature is of benefit to electric transport, compared to the granular carbons.[36] Meanwhile, the HRTEM image demonstrates the amorphous structure of the KOH-activated carbon material, which is consistent with previous reports on hard carbon derived from the pyrolysis of the carbonaceous precursor.[37-38] Therefore, these porous carbon materials derived from ox horn could be promising electrode materials for lithium ion batteries.

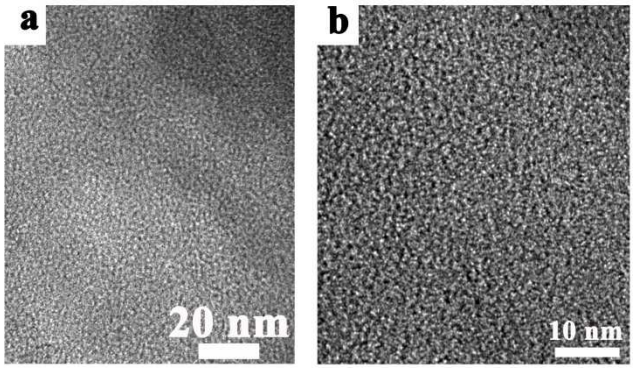

Fig. 4 (a and b) HRTEM images of carbon material with KOH treatment.

To analyze the elemental composition and bonding configurations, XPS was performed on the as-obtained product. The XPS spectrum of the OHC derived from KOH treatments (Fig. 5a) possess three peaks centered at 284.8 eV, 400.0 eV and 513.4 eV, corresponding to C 1s, N 1s and O 1s, respectively. The peak assignment and the percentage of chemical composition are summarized in Table 1. The XPS spectrum of the C 1s (Fig. 5b) can be divided into three peaks. The main peak at 284.8 eV is identified to the sp^2 hybridized C-C. The weak peaks at 285.9 eV and 288.1 eV can be related to correspond to C-N, O=C-O groups respectively. [26, 39, 40] Nitrogen (3.5) has a higher electronegativity than carbon (3.0), because its atomic diameter is smaller. Meanwhile, there is a stronger interaction between Li and the N-doped carbon material because of the hybridization of nitrogen lone pair electrons with the π electrons in the carbon. Therefore, the electronegativity and hybridization might be favorable for lithium insertion.[41, 42] As shown in Fig. 5c, it shows the N 1s spectrum, which can be deconvoluted into three individual peaks, locating at 398.4 eV, 399.7 eV, 400.9 eV, and 402.3 eV corresponding to pyridinic, pyrrolic, graphitic nitrogen, and pyridine-N-oxide respectively.[24, 41, 42] It should be pointed out that pyridinic N is more favorable than pyrrolic-N for Li storage and is a significant factor in the improvement of reversible capacity.[24, 42] From table 1, it can be seen that the mass percentage of doped nitrogen is as high as 5.5% of product. The high nitrogen content in the carbon materials is beneficial to the formation of defects and the enhancement of electric conductivity, which can both improve the electrochemical performance of the anode materials. The O1s spectrum contains three peaks at 531.2, 532.3 and 533.5 eV, corresponding to the presence of different oxygen functionalities such as C=O, O-C-O, O=C-O respectively. The oxygen mainly arises from the thermally stable groups in the carbon except for that of oxygen or water absorbed on the carbon surface.

To further determine the qualitative composition of the as-fabricated OHC, FTIR spectroscopy was carried out (Fig. S1, ESI†). As can be seen, the bands located within a range 3250-3550 cm^{-1} is assigned to N-H and O-H stretching vibrations.[43] The peaks at 2350 cm^{-1} implied the existence of CO_2, which may be absorbed on the surface of carbon materials. The wide adsorption bands at 1092 cm^{-1} is attributed to the C-O groups in ethers or phenols. Moreover, The N-doping could be proved by the presence of adsorption peaks at about 1250 cm^{-1}(assigned to the C-N stretching vibration) and 1550 cm^{-1}(assigned to pyridinic N or pyrrolic N groups).[44] At the same time, elemental analysis (Table S1, ESI†) indicates that the N and H contents of the as-synthesized carbons (OHC) were 5.4% and 3.5%, respectively. It should be pointed out that the existence of N atoms creates a large number of defects in the carbon material and produces more active sites for Li storage.[24] The high-level nitrogen doping can also restrain the electrolyte decomposition and surface side reactions of the electrodes with the electrolyte, reduce the formation of the SEI film.[20] In addition, appropriate hydrogen contents in the carbon fragment may make a contribution to the excess reversible capacity.[31, 45] In this case, hydrogen may work as an electro acceptor ($Li^{\delta+}$…$H^{\delta-}$).

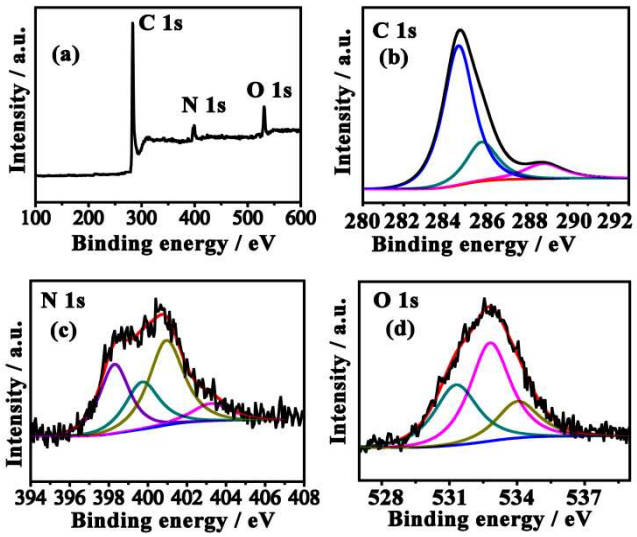

Fig. 5 The total XPS spectrum (a) and the C 1s (b), the N 1s (c) and the O 1s (d) spectra of the OHC.

Table 1 Peak assignment of C1s, N1s and O1s of the fabricated OHC.

Peak	Binding energy (eV)	Assignment	Atom %
C 1s	284.8	sp^2 C-C	
	285.9	C-N	87.6
	288.1	O=C-O	
N 1s	398.4	Pyridinic nitrogen	
	399.7	Pyrrolic nitrogen	5.5
	400.9	Graphitic nitrogen	
	402.3	Pyridine-N-oxide	
O 1s	531.2	C=O	
	532.3	O-C-O	6.9
	533.5	O=C-O	

Coin-type cells were assembled to assess the electrochemical performance of the OHC. CV curves were recorded at the voltage range of 0.01–3.0 Vat a scanning rate of 0.1 mV s^{-1} (Fig. 6), the OHC electrode displays typical CV curves of the carbonaceous anode materials.[24] As can be seen in Fig. 6b, the carbon material derived from ox horns without KOH treatment presented a low specific discharge and charge capacities, only 283, 278 mA h g^{-1} after 50th cycles. In comparison with the performances of carbon without KOH treatment, the OHC shows a much higher reversible capacity. As depicted in Fig. 6b, the OHC delivers large initial charge and discharge capacities of 1290 and 2166 mA h g^{-1} respectively, but with a low coulombic efficiency of 59.5%. It should be pointed out that the initial reversible capacity for the OHC is more than three times higher than that of pure carbon, revealing that there may be some other lithium storage routes existing in OHC except the conventional graphite intercalation mechanism.[45, 46] The large loss in capacity during the first cycle means that a significant part of the lithium is unavailable for reversible reactions. Broadly speaking, the large initial capacity fading can be attributed to the conversion of the carbon electrode from its pristine form to an active lithium storage host; the formation of a solid electrolyte interface (SEI) caused by the catalytic reduction of the electrolyte components on the active electrode surface, and/or irreversible lithium insertion into special positions such as in the vicinity of residual H atoms in the carbon material as it was previously reported in the literature.[22, 47] Although the large irreversible capacity loss was observed in the first cycle, the coulombic efficiency of OHC was significantly enhanced in the sequent cycles. From the Fig. 6c, the reversible capacity of the OHC in the 2nd cycle was 1231 mA h g^{-1} and the coulombic efficiency increases dramatically to 94%. Even at 50th cycle, a steady state reversible capacity of 1181 mA h g^{-1} has been achieved at 100 mA g^{-1}, which shows a good electrochemical property. Fig. 6d presented the galvanostatic charge–discharge curves of the OHC for the 20th cycle at current rates ranging from 100 mA g^{-1} to 5 A g^{-1} between the voltages of 0.01 and 3.0 V. The capacity drops with the increase of current densities, indicating that the capacity loss is limited by lithium-ion diffusion. At a low current density of 100 mA g^{-1} (1 C = 372 mA g^{-1}), the reversible capacity of OHC was 1181 mA h g^{-1}. It should be noted that the OHC exhibits a high-rate capability of 304 mA h g^{-1} at 5 A g^{-1}, which shows a superior rate performance.

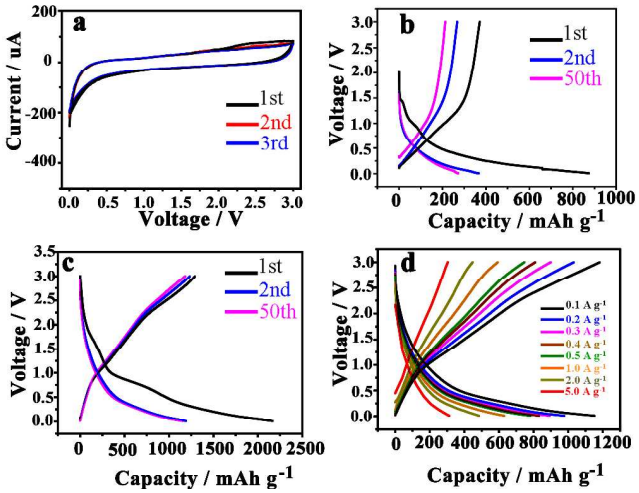

Fig.6 (a) cyclic voltammograms (CV) of OHC at a scan rate of 0.1 mV s^{-1} for the initial three cycles, galvanostatic charge and discharge profiles of the NOHC (b) and OHC (c) at 100 mA g^{-1} between 0.01 V and 3.00 V for the 1st, 2nd and 50th cycles, and (d) charge/discharge curves of the OHC for the 20th cycle at various current densities.

To further verify the performance of OHC anode for high rate applications, rate capability behavior was tested with different current densities such as 0.1, 0.2, 0.3, 0.4, 0.5, 1, 2 and 5 A g^{-1}. The carbon electrode shows a reversible capacity of 1181, 1031, 898, 808, 750, 592, 470 mA h g^{-1} at 0.1, 0.2, 0.3, 0.4, 0.5, 1, 2 A g^{-1}, respectively. Even at extremely high current density 5 A g^{-1} (13.4 C), the reversible capacity are still as high as 304 mA h g^{-1}. When the rate is turned back to 0.1 A g^{-1} after cycling at different current rates, the capacity can be recovered (1179 mA h g^{-1}), implying a good reversibility of the material. In addition to the good rate performance, the cycling performance of KOH-activated carbon electrode was also evaluated at 0.1 and 1 A g^{-1} respectively. As presented in Fig.7b, a satisfactory cycling performance was observed, being as high as 1178 mA h g^{-1} and 591 mA h g^{-1} at 0.1 and 1 A g^{-1} respectively even after 100 cycles. To the best of our knowledge, OHC anode delivers high reversible capacity and superior rate performance compared with most carbon materials derived from various biomass sources (Table S2, ESI†). The unique porous structure and the large amount of defects with nitrogen-doping jointly contribute to the electrochemical performances of OHC.

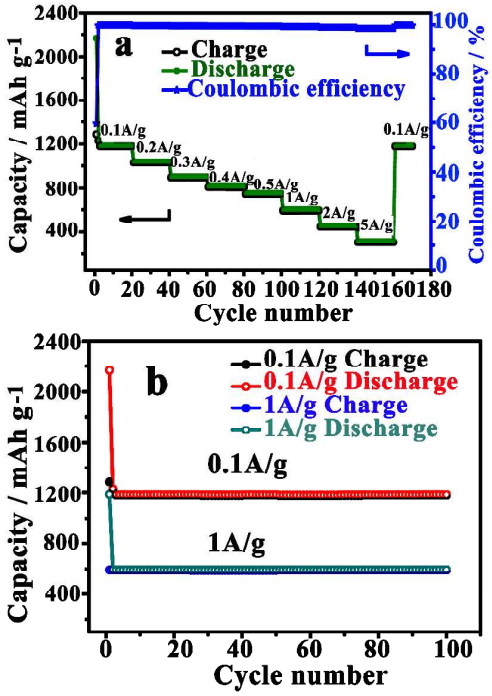

Fig.7 (a) charge-discharge cycling performances of OHC at different current densities from 0.1 A g^{-1} to 5 A g^{-1} at room temperature and (b) Cycling capability of OHC at current densities of 0.1 A g^{-1} and 1 A g^{-1}.

EIS is an important tool to understand this surface-dependent LIBs performance. In order to further investigate the transport kinetics for the good electrochemical performances of OHC, EIS measurements were conducted after 10, 20, 50, and 100 cycles at a current density of 100 mA g^{-1}. As depicted in Fig. 8, the Nyquist plots for OHC consist of a depressed semicircle in the high and middle frequency regions and a straight line in the low frequency region. In the equivalent circuit, R_e is the total resistance of the electrolyte, electrode and separator, CPE 1 and R_f are the surface film capacitance and the resistance for lithium ion migration through the SEI film, respectively. In addition, CPE 2 and R_{ct} are the double layer capacitance and charge transfer resistance, respectively; Z_w is the Warburg impedance related to the lithium ion diffusion in the inserted materials; and C1 is related to the insertion capacitance reflecting the occupation of lithium into the inserted sites.[48-49] It can be seen that the diameters of the semicircles decrease gradually with increasing cycle numbers, revealing depressed resistances. This is a very interesting phenomenon and has rarely been reported in the literatures.[50] The EIS is modeled by an equivalent circuit shown in Fig. 8b, and the obtained kinetic parameters of OHC are summed up in Table 2. Generally speaking, a high surface area results in more side reactions that thicken the SEI film. However, the value of R_f remained stable with enhancing cycle numbers, meaning that the lithium ions in the OHC can stably pass through the SEI film. This phenomenon could be attributed to the appropriate nitrogen content of OHC, which could suppress the electrolyte decomposition and surface side reactions of the electrodes with the electrolyte, favoring the formation of the stable SEI film.[9] From the table 2, the value of R_{ct} gradually decrease with the cycle process. It results from the large surface area and defects from N-doping, which may lead to large irreversible lithium insertion into the electrodes with the increase of cycle numbers.[51] This process may result in the improvement of electrical conductivity in the electrode of OHC. In addition, the exchange current density i_0 exchange current density (i_0) is one of key parameters that influences the rate of a charge transfer controlled electrochemical reaction and can be calculated according to equation $i_0 = RT/nFR_{ct}$, [52] where R is the gas constant, T is the absolute temperature, n is the number of transferred electrons and F is the Faraday constant. As seen in Table 2, the i_0 gradually increases with the cycle process, demonstrating a favorable charge transfer process of lithium ion insertion/extraction reaction. These results indicate that the suitable nitrogen doping combined with its unique interconnected pore structure can afford lithium ions stable diffusion channels, leading to a superior electrochemical performance.

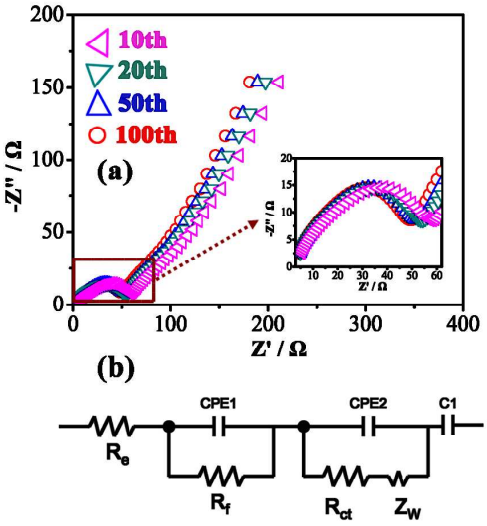

Fig.8 (a) Typical Nyquist plots of OHC electrodes after different cycles, (b) equivalent circuit for an OHC electrode.

Table 2 Kinetic parameters of an OHC electrode after different cycles.

Cycle	R_e (Ω)	R_f (Ω)	R_{ct} (Ω)	i_0(mA cm^{-2})
10th	3.81	11.35	41.84	0.614
20th	3.85	11.27	39.88	0.644
50th	3.77	11.24	37.99	0.676
100th	3.72	11.21	35.07	0.732

In order to determine the morphology and structure of the OHC, batteries after 20 cycles running at the current density of 0.1 A g^{-1} were disassembled, and the carbon anodes were immersed in dimethyl carbonate (DMC) to remove the residual electrolyte for TEM. For clear comparison, Fig. S2 (ESI†) shows the TEM images of the porous carbon before (Fig.S2a, S2c) and after cycling (Fig. S2b, S2d). In the presence of acetylene black and binder, it clearly shows that the structure does not change significantly after 20 cycles (compared to Fig. S2a, S2c), which confirms that the structure is stable in the repetitive Li-ion insertion and extraction process. This agrees well with the previous results that the carbon with a large specific surface area and high porosity did not change its structure significantly after lithiation.

The high reversible capacity and rate capability for OHC can be ascribed to the following reasons. On one hand, the large specific surface area facilitates good contact of the electrode of OHC with electrolyte and further promotes the transportation of lithium ions; the numerous pores may not only act as reservoirs for storage of lithium ions, but also accommodate the local volume change of the carbon anode material, thus effectively relieving the pulverization issues and leading to a good cycling ability. [21, 53, 54] As shown in Fig. 9, the material possesses a hierarchical porous structure with the coexistence of micropores and mesopores, which afford facile storage and transport channels for lithium-ions. Specifically, large quantities of micropores can act as charge accommodation which is essential for super-high capacity. Small amount of mesopores in OHC can shorten the diffusion length of the lithium ions by the formation of ion-buffering reservoirs, and provide a high surface area which helps to enlarge the contact area between the electrolyte and the electrode, thereby increasing the number of active sites of the insertion and extraction of the lithium ion.[54] On the other hand, the interconnected pores provide a continuous pathway for electron transport. Moreover, nitrogen-doping generates a large number of structural defects that promote rapid charge-transfer reactions and act as lithium insertion sites for storage of lithium-ions and make an additional contribution to the exceptional performance.

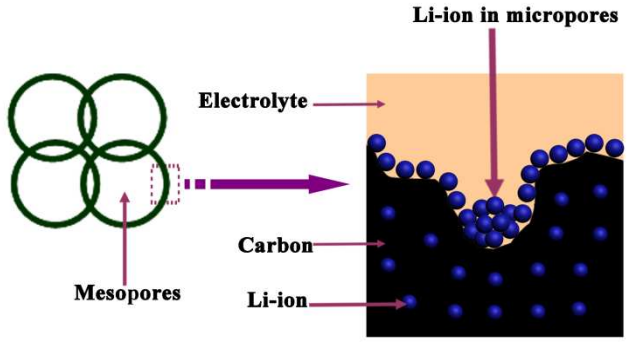

Fig.9 Schematic representation of Li-ion storage in OHC.

4. Conclusions

In this work, nitrogen-rich porous carbon has been successfully fabricated from ox horn by a facile, economical and effective method. The as-synthesized OHC employed as an anode material for LIBs delivered a large reversible lithium storage capacity (1178 mA h g^{-1} in the 100th cycle at 0.1 A g^{-1}) and a superior rate capability (304 mA h g^{-1} when the discharge current increased from 0.1 A g^{-1} to 5 A g^{-1}), revealing great potential as an anode material for high-performance LIBs. The excellent electrochemical performances could be ascribed to the unique porous structure, the large specific surface area, and the appropriate nitrogen introduction (5.5%) in the porous carbon. This approach can be mass-produced and the time of immersing process can be expected to reduce by increasing the KOH solution temperature. Furthermore, owing to the high nitrogen content and the hierarchical pore structure, OHC can also be applied in catalysis, supercapacitors, adsorbents and fuel cells.

Acknowledgements

We greatly appreciate the Natural Science Foundation of China (21275104, 21177090 and 21175094) for supporting this work.

Notes and references

[a] *College of Chemical Engineering, Sichuan University, No.24 South Section 1, Yihuan Road, Chengdu 610065, PR China. Fax: +86-28-85412907; Tel: +86-28-85416218*
[b] *Institute of New Energy and Low-Carbon Technology, Sichuan University, No.24 South Section 1, Yihuan Road, Chengdu 610065, PR China. Fax:+ 86-28-6213-8325; Tel: +86-28-6213-8375*
[c] *College of Chemistry, Sichuan University, 29 Wangjiang Road, Chengdu 610064, PR China. Fax: +86-28-85416029; Tel: +86-28-85416029*
**Corresponding author: Dan Xiao; E-mail: xiaodan@scu.edu.cn;*

References

1 J. M. Tarascon, M. Armand, *Nature*, 2001, **414**, 359.
2 J. R. Dahn, T. Zheng, Y. Liu and J. S Xue, *Science*, 1995, **270**, 590.
3 M. Winter, O. J. Besenhard, M. E. Spahr and P. Novak, *Adv. Mater.*, 1998, **10**, 725.
4 M. Armand and J. M. Tarascon, *Nature*, 2008, **451**, 652.
5 B. J. Landi, M. J. Ganter, C. D. Cress, R. A. DiLeo, R. P. Raffaelle, *Energy Environ. Sci.*, 2009, **2**, 638.
6 C. Li, X. Yin, L. Chen, Q. Li, T. Wang, *J. Phys. Chem. C*, 2009,**113**,13438.
7 H. Wang, T. Abe, S. Maruyama, Y. Iriyama, Z. Ogumi, K. Yoshikawa, *Adv. Mater.*, 2005, **17**, 2857.
8 F. D. Han, Y. J. Bai, R. Liu, B. Yao, Y. X. Qi, N. Lun, J. X. Zhang, *Adv. Energy Mater.*, 2011, **1**, 798.
9 Z. S. Wu, W. Ren, L. Xu, F. Li, H. M. Cheng, *ACS Nano*, 2011, **5**,5463.
10 E. Peled, V. Eshkenazi, Y. Rosenberg, *J. Power Sources*, 1998, **76**, 153.
11 S. H. Guo, J. H. Peng, W. Li, K. B. Yang, L. B. Zhang, S. M. Zhang, H. Y. Xia, *Appl. Surf. Sci.*, 2009, **255**, 8443.
12 W. Z. Shen, Z. F. Qin, H. G. Wang, Y. H. Liu, Q. J. Guo, Y. L. Zhang , *Colloids Surf. A*, 2008, **316**, 313.
13 Y. J. Hwang, S. K. Jeong, K. S. Nahm, J. S. Shin, A. M. Stephan, *J. Phys. Chem. Solids*, 2007, **68**, 182.
14 A. M. Stephan, T. P. Kumar, R. Ramesh, S. Thomas, A. K. Jeong, K. S. Nahm, *Mater. Sci. Eng. A*, 2006, **430**, 132.
15 L. Wang, Z. Schnepp, M. M. Titirici, *J. Mater. Chem. A*, 2013, **1**, 5269.
16 F. Zhang, K. X. Wang, G. D. Li and J. S. Chen, *Electrochem.*

Commun., 2009, **11**, 130.
17 X. L. Wu, L. L. Chen, S. Xin, Y. G. Guo, Q. S. Kong, Y. Z. Xia, *ChemSusChem*, 2010, **3**, 703.
18 J. C.Arrebola, A. Caballero, et al., *J. Electrochem.Soc.*, 2010, **157**, A791.
19 Y. J Hwang, S. K. Jeong, K. S. Nahm, J. S. Shin and A. M. Stephan, *J. Phys. Chem. Solids*, 2007, **68**, 182.
20 L. Chen, Y. Z. Zhang, C. H. Lin and D. Xiao, *J. Mater. Chem. A*, 2014, **2**, 9684.
21 L. Qie, W. M. Chen, Z. H. Wang, Q. G. Shao, X. Li, L. X. Yuan, X. L. Hu, W. X. Zhang and Y. H. Huang, *Adv. Mater.*, 2012, **24**, 2047.
22 Y. S. Hu, P. Adelhelm, B. M. Smarsly, S. Hore, M. Antonietti and J. Maier, *Adv. Funct. Mater.*, 2007, **17**, 1873.
23 Y. P. Wu, S. B. Fang and Y. Y. Jiang, *J. Mater. Chem.*, 1998, **8**, 2223.
24 Z. Li, Z. W. Xu, X. H. Tan, H. L. Wang, C. M. B. Holt, T. Stephenson, B. C. Olsen and M. Mitlin, *Energy Environ. Sci.*, 2013, **6**, 871.
25 B. M. Way and J. R. Dahn, *J. Electrochem. Soc.*, 1994, **141**, 907.
26 W. J. Qian, F. X. Sun, Y. H. Xu, L. H. Qiu and F. Yan, *Energy Environ. Sci.*, 2014, **7**, 379.
27 K. R. Saravanan, N. Kalaiselvi, *Carbon*, 2014, **81**, 43.
28 J. K. Ou, Y. Z. Zhang, L. Chen and D. Xiao, RSC Advances, 2014, 4, 63784.
29 R. J. White, V. Budarin, etal. *Chemical Society Reviews*, 2009, **38**, 3401.
30 K. T. Lee, J. C. Lytle, N. S. Ergang, S. M. Oh, A. Stein, *Adv. Funct. Mater.*, 2005, **15**, 547.
31 D. Y. Pan, S. Wang, B. Zhao, M. H. Wu, H. J. Zhang, Y. Wang and Z. Jiao, *Chem. Mater.*, 2009, **21**, 3136.
32 Y. Liu, J. X. Xue, T. Zhang and J. R. Dahn, *Carbon*, 1996, **34**, 193.
33 H. L. Wang, Q. M. Gao and J. Hu, *J. Am. Chem. Soc.*, 2009, **131**, 7016.
34 A. Ferrari and C. J. Robertson, *Phys. Rev. B: Condens. Matter Mater. Phys.*, 2000, **61**, 14095.
35 F. Tuinstra and J. L. Koenig, *J. Chem. Phys.*, 1970, **53**, 1126.
36 F. Cheng, Z. Tao, J. Liang and J. Chen, *Chem. Mater.*, 2008, **20**, 667.
37 L. Qie, W. M. Chen, H. H. Xu, X. Q. Xiong, Y. Jiang, F. Zou, X. L. Hu, Y. Xin, Z. L. Zhang and Y. H. Huang, *Energy Environ. Sci.*, 2013, **6**, 2497.
38 H. G. Wang, Z. Wu, F. L. Meng, D. L. Ma, X. L. Huang, L. M. Wang and X. B. Zhang, *ChemSusChem*, 2013, **6**, 56.
39 W. Jang, C. E. Lee, S. C. Lyu, T. J. Lee and C. J. Lee, *Appl. Phys. Lett.*, 2004, **84**, 2877.
40 D. C. Wei, Y. Q. Liu, Y. Wang, H. L. Zhang, L. P. Huang and G. Yu, *Nano Lett.*, 2009, **9**, 1752.
41 W. H. Shin, H. M. Jeong, B. G. Kim, J. K. Kang, J. W. Choi, *Nano Lett.*, 2012, **12**, 2283.
42 C. C. Ma, X. H. Shao and D. P. Cao, *J. Mater. Chem.*, 2012, **22**, 8911.
43 Z. Yang, H. Q. Wu, B. Simard, *Electrochem. Commun.*, 2002, **4**, 574.
44 G. P. Hao, W. C. Li, D. Qian, A.H. Lu, *Adv. Mater.*, 2010, **22**, 853.
45 N. A. Kaskhedikar, J. Maier, *Adv. Mater.*, 2009, **21**, 2664.
46 L. Su, Z. Zhou, P. Shen, *J. Phys. Chem. C*, 2012, **116**, 23974.
47 G. Ji, Y. Ma and J. Y. Lee, *J. Mater. Chem.*, 2011, **11**, 9819.
48 J. Yi, X. Li, S. Hu, W. Li, L. Zhou, M. Xu, J. Lei and L. Hao, *J. Power Sources*, 2011, **196**, 6670.
49 D. Lu, W. Li, X. Zuo, Z. Yuan and Q. Huang, *J. Phys. Chem. C*, 2007, **111**, 12067.
50 S. B. Yang, H. H. Song, X. H. Chen, A. V. Okotrub and L. G. Bulusheva, *Electrochim. Acta*, 2007, **52**, 5286.
51 R. R. Song, H. H. Song, J. S. Zhou, etal. *J. Mater. Chem.*, 2012, **22**, 12369
52 G. D. Li, L. Q. Xu, Q. Hao, M. Wang, Y. T. Qian, *RSC Advances*, 2012, **2**, 284.
53 L. Ji, Z. Lin, M. Alcoutlabi, X. Zhang, *Energy Environ. Sci.*, 2011, **4**, 2682.
54 D. W. Wang, F. Li, M. Liu, G. Q. Lu and H. M. Cheng, *Angew. Chem., Int. Ed.*, 2008, **47**, 373.

Graphical for abstract

The OHC derived from ox horn shows superior performance as an anode material for LIBs with high reversible capacity (1181 mA h g^{-1} at 0.1 A g^{-1}) and excellent rate capability (304 mA h g^{-1} at 5 A g^{-1}).